

Regional climate model simulation of soil moisture and its application in drought reconstruction across China from 1911 to 2010

Aihui Wang  | Xianghui Kong

Nansen-Zhu International Research Centre, Institute of Atmospheric Physics, Chinese Academy of Sciences, Beijing, P. R. China

Correspondence

Aihui Wang, Nansen-Zhu International Research Centre, Institute of Atmospheric Physics, Chinese Academy of Sciences, P.O. Box 9804, Beijing 100029, P. R. China.
Email: wangaihui@mail.iap.ac.cn

Funding information

National Key Research and Development Project of China, Grant/Award Number: 2016YFA0602401; National Natural Science Foundation of China, Grant/Award Number: 41925021 & 41875106

Abstract

Regional climate model has been widely used to simulate terrestrial water cycles, but its simulations used in the long-term agriculture drought reconstruction have not been investigated in China. This study presents an analysis of soil moisture (SM) drought in China during 1911–2010 on the basis of the simulations from the Weather Research and Forecasting (WRF) model driven by two twentieth century reanalysis products. Comparisons of modelled SM with station observations indicate that WRF has certain capability in reproducing its magnitudes and temporal variabilities. Model performance are greatly impacted by lateral boundary conditions. The average SM derived from two experiments is closer to observations than the individual one and thus they are then applied in drought investigation. During the study period, SM shows a wetting tendency from northwestern to central eastern China, while it displays a drying tendency in the northeast, western Tibetan Plateau, and part of southeastern China. The spatial pattern of number drought events resembles that of annual precipitation, showing an increasing tendency from northwestern (arid) to southeastern (humid) regions. In arid regions, drought events are generally prolonged and frequent but less severe. In humid regions, in contrast, drought events usually persist less than 6 months and are less frequent but relatively severe. During the examined 100-year period, roughly 28.4, 28.9 and 38.4% of land areas in China show significant trends for duration, severity, and frequency, respectively ($p > .8$). Both drought duration and severity show decreasing tendencies in vast regions, and the land areas showing increased drought frequency is slightly less than that of areas showing its decreased tendency. This study is a first attempt to apply regional climate modelling to investigate a centennial long SM change in China and presents a new way to explore long-term drought characteristics and their changes.

KEY WORDS

centurial long, drought, soil moisture, variability, WRF

1 | INTRODUCTION

Drought is a frequently occurring natural hazard that leads to great economic losses and environmental impacts (Below *et al.*, 2007). For example, a severe drought occurring in winter–spring of 2011 in southern China destroyed more than 98.9 million hectares of crops and affected more than 4.9 million people and 3.4 million livestock (Sun and Yang, 2012). Drought can occur on multiple scales. Its time scale varies from several days to decades, and its spatial scale can be local or extend to thousands of square kilometres (Qian *et al.*, 2003; Shen *et al.*, 2007; Dai, 2011; Wang *et al.*, 2016). Drought has occurred more frequent and prolonged over regional and global land areas in past decades (e.g., Sheffield *et al.*, 2009; Dai, 2011) and it is also projected to be more severe under climate change scenarios in China (Chen and Sun, 2017) and in Europe (Spinoni *et al.*, 2018). Su *et al.* (2018) showed that the drought loss would be increased 10 times under 1.5°C warming level as compared to 1986–2005 reference period and it will be double under extra 0.5°C warming. Understanding of the occurrence and evolution of historical drought events can provide knowledge for future drought prediction and projection.

In past decades, researchers have proposed various definitions for droughts, for example, “a period of abnormally dry weather sufficiently prolonged for the lack of precipitation to cause a serious hydrological imbalance” (WMO 1992); “insufficient water to meet needs” (Redmond, 2002); and “a dry spell relative to its local normal condition” (Dai, 2011). The above definitions refer to a deficiency of water, including precipitation (Pr), runoff (Ro), soil moisture (SM), and virtual water shaped by socioeconomics, that occurs for a period of time. Those three quantities are sequentially used to represent the meteorological drought, hydrological drought, and agriculture drought, respectively. Among these, SM plays an important role in ecosystem lifecycles and human activities and its below-normal condition within a region during a period of months to years will directly lead to agricultural drought and result in reduced crop production. The impacts of SM drought on crop production can be explained by transpiration, which transports water and nutrition from soil and then through vegetation root and foliage to atmosphere (Gupta *et al.*, 2020). Water for transpiration firstly comes from the internal plant storage and then from SM in the root zone. Under the drier soil condition, the water potential of soil is relatively lower and the root is unable to suck enough water from surrounding soils (Bonan, 2002). As a consequence, the crop cannot obtain enough water to sustain plant growth, which then decreases the yield.

China covers a vast land area, and its climate varies from tropical in the south to the temperate in the north and from humid in the east to arid in the northwest. According to the Chinese National Statistical database for 1980–2018, drought accounts for over 65% of economic losses resulting from all meteorological hazards, and it affects roughly 50% of China's land area every year (<http://data.stats.gov.cn>). China is also a large agricultural country with agricultural areas currently occupying more than 500 million square kilometres. During the 20th century, China experienced agricultural restructuring along with intensified climate change, especially since the 1980s in the north China (Wang *et al.*, 2018). Studies have reported that the East Asian Summer Monsoon system, the main factor shaping climate patterns in China, has decadal variability (Wang, 2001; Ding *et al.*, 2018). These changes should also impact the long-term evolution and variability of SM in China. Thus, it is needed to take insight into the variability in SM drought patterns in China during the entire 20th century. Investigation of drought patterns over longer periods will be very helpful in establishing policies for climate change mitigation and adaptation.

However, most studies on SM drought in China focus on the most recent decades (i.e., the last 30–50 years) and few of them have addressed these events for prolonged periods (e.g., Wang *et al.*, 2011; Huang *et al.*, 2016). This is mainly attributable to an absence of reliable long-term SM datasets. SM is usually obtained directly through in situ measurement, satellite observations, and/or numerical model simulations (Wang and Zeng, 2011; Yang, 2013; Wang and Shi, 2019). In the past 40 years, remotely-sensed SM datasets have been widely used in drought investigations due to their extensive spatial coverage and continuous temporal extent (e.g., Rhee *et al.*, 2010; Liu *et al.*, 2019), but they only represent moisture conditions within the upper 2–5 cm soil layers and are only reliable for bare and sparsely vegetated regions (Liu *et al.*, 2011). On the other hand, SM products derived from offline land surface model (LSM) simulations have been widely used in regional and global drought research (Sheffield *et al.*, 2009; Wang *et al.*, 2009, 2011). For instance, Sheffield *et al.* (2009) identified global drought trends and variability in the second half of the twentieth century using a SM dataset derived from a hydrological model experiment. Wang *et al.* (2011) ran four land surface models (LSMs) driven by the atmospheric forcing dataset derived from reanalysis products and observations for China for 1950–2006, and the simulated SM ensemble median was then used to successfully reconstruct drought characteristics for the studied period. However, offline LSM simulations usually require the use of atmospheric forcing variables with space–time

continuity at a subdaily resolution, most of which were not constructed before the 1950s. Drought characteristics (i.e., intensity, duration, and trends) depend on the time period of interest, which is often restricted to the data availability. The centurial long SM datasets over large regions can only be obtained from numerical model outputs. Moreover, meteorological drought may prevail over large regions or even across continents while SM drought is largely heterogeneous at regional scales and its investigation requires datasets with relatively fine spatial resolutions.

Taking into account the above concerns, the regional climate model (RCM) is one of the best tools for retrospectively simulating SM in China. Compared to global climate models (GCMs), one of the greatest advantages of the RCM concerns the fact that it enhances descriptions of physical processing over complex territories and offer the added value of climate variables (Gao *et al.*, 2011; Giorgi, 2019; Kong *et al.*, 2019). RCMs necessitate the use of lateral boundary meteorological variables surrounding the modelling domain, which are usually derived from GCM outputs or global reanalysis products. Reanalysis products have merged both climate model simulations and observational information, and they have been extensively used for initial and lateral boundary conditions in numerous RCM modelling experiments (e.g., Xue *et al.*, 2014; Kong and Bi, 2015; Gao *et al.*, 2017; Giorgi, 2019; Kong *et al.*, 2019). Globally, several institutions provide continuous reanalysis products. Among them, two reanalysis products have extent to more than 100 years: the NOAA Twentieth Century Reanalysis (20CR) (Compo *et al.*, 2011) and ECMWF Twentieth-Century Reanalysis products (ERA-20C, Poli *et al.*, 2016). Kong and Bi (2015) found that the WRF simulations generally reduced air temperature biases and better reproduced the magnitude and positioning of heavy rain relative to those in the driven 20CR reanalysis. Kong *et al.* (2019) further reported that both RegCM4 and WRF driven by ERA-20C reanalysis products can effectively reproduce temperature extremes in China although both models exhibit varied performance in terms of specific variables. The inputs of RCMs require the use of several climate variables at different vertical levels and most cannot be observed and validated. Because assimilation systems, observation datasets, and climate models vary across institutions and research centres, no reanalysis products are superior to others in terms of all of the above climate variables (e.g., Wang and Zeng, 2012). Therefore, using multiple reanalysis products to drive a state-of-art RCM might be a practical means to produce reliable SM datasets.

Since the soil water holding capacity and soil texture differ from region to region (e.g., Shangguan *et al.*, 2013), the magnitudes of SM (in volumetric form) is

heterogeneous across space (Wang and Shi, 2019). Wang *et al.* (2009, 2011) converted the original model-simulated monthly SM to a percentile (SMP) with respect to its climatology for the same month during their study period and then successfully applied the SMP to identify drought in the continental United States and China, respectively. The SMP magnitudes in all land pixels are within range of 1–100%, facilitating the comparison of different climatic regimes and periods. Similar approach has been used in other studies (e.g., Sheffield *et al.*, 2009). Moreover, the SMP removes the effect of seasonal cycles and allows drought analyses to focus on the variations of interannual or longer time scales. In previous studies (Sheffield *et al.*, 2009; Wang *et al.*, 2009, 2011), the occurrence of drought is defined as that SMP is equal to or less than 20% at each grid cell, which implies that a drought would have a 5-year return period if SMP is evenly distributed during the study period. Reducing this threshold would lengthen the drought return period. In this study, to investigate SM drought characteristics and their evolution in China for the entire 20th century, we run WRF driven by both 20CR and ERA-20C. The simulated monthly SM datasets are evaluated with in situ measurements in China. Based on our evaluations, a drought index is constructed based on the average SM values generated from two experiments and it is then used to identify drought events occurring from 1911 to 2010. The spatial pattern and temporal evolution of SM drought events are then analysed. The study explores: i) the performance of SM reproduced by WRF is driven by two reanalysis products, and ii) the characteristics and evolutionary of SM drought in China over a 100-year period. Section 2 briefly describes the structure and physical configuration of WRF model, specifically on SM-related processes, Section 3 introduces two reanalysis products and methods used to define and analyse drought characteristics, Section 4 illustrates the validation of WRF-simulated SM data, Section 5 presents the analyses of SM drought characteristics, and conclusions are summarized in Section 6.

2 | MODEL AND DATA

2.1 | WRF model and experiments

The Advanced Research WRF model (WRF-ARW; Skamarock *et al.*, 2008) version 3.6.1 was used to perform simulations for China. The model's configurations are described in detail in Kong and Bi (2015) and Kong *et al.* (2019). Here, we briefly introduce these physical schemes with an emphasis on land surface processes, especially for SM-related processes. Physical parameterization schemes include the QNSE-EDMF for PBL

(Sukoriansky *et al.*, 2006), the Goddard scheme for the transformation of radiation (Chou and Suarez, 1999), the WSM6 scheme for microphysics (Hong and Lim, 2006), and the SAS scheme for convection (Han and Pan, 2011). The NOAH LSM is a land surface scheme (Chen and Dudhia, 2001) and has been reported to comprehensively represent land surface hydrological and heat processes in many studies (e.g., Xia *et al.*, 2014).

The NOAH LSM used in the WRF consists of four soil layers: 0–10, 10–40, 40–100 and 100–200 cm from top to bottom, and both soil liquid and solid water are calculated at the middle of each soil layer (i.e., 5, 25, 70 and 150 cm from the soil surface). Water movement between soil layers is controlled by the Richards equation (Richards, 1931), and soil ice is parameterized based on soil temperature in the NOAH LSM (Chen and Dudhia, 2001). In this study, the total soil water was defined as the summation of soil liquid water and soil ice at each time step in each layer. We computed the monthly mean model-simulated total SM, and this was then used to perform the following analyses.

Using the above model configurations, two century-long WRF experiments were performed driven by forcing fields from the 20CR (Compo *et al.*, 2011) and ERA-20C (Poli *et al.*, 2016) reanalysis products, respectively. The 20CR products were generated by NOAA using available surface pressure observations as the only input in the assimilation system, and they have been demonstrated to effectively represent tropospheric temperature relative to radiosonde observations (Compo *et al.*, 2011). The ERA-20C was developed by the ECMWF and assimilates both surface pressure and marine wind observations (Poli *et al.*, 2016). The 20CR products are available from 1850 onwards, while the ERA-20C products are between 1900 and 2010.

The WRF model domain was centred at (36°N, 105°E) with a 50 km × 50 km horizontal resolution and extent of 139 (latitude) × 119 (longitude) grid points, covering most of the continental East Asia (Figure 1a). The experiments were conducted for January 1, 1900 to December 31, 2010 with default model initial land surface settings. In the following sections, simulations driven by ERA-20C and 20CR are referred as WRF-ERA20C and WRF-20CR, respectively. To reduce initialization impacts, the first 11 years of the simulations are treated as a spin-up period, and the simulated monthly SM for 1911–2010 (100 years) within the continuous China domain were used to perform drought analyses.

2.2 | Observations

Wang and Shi (2019) (hereafter referred as to WS2019) processed and analysed in situ measured SM dataset

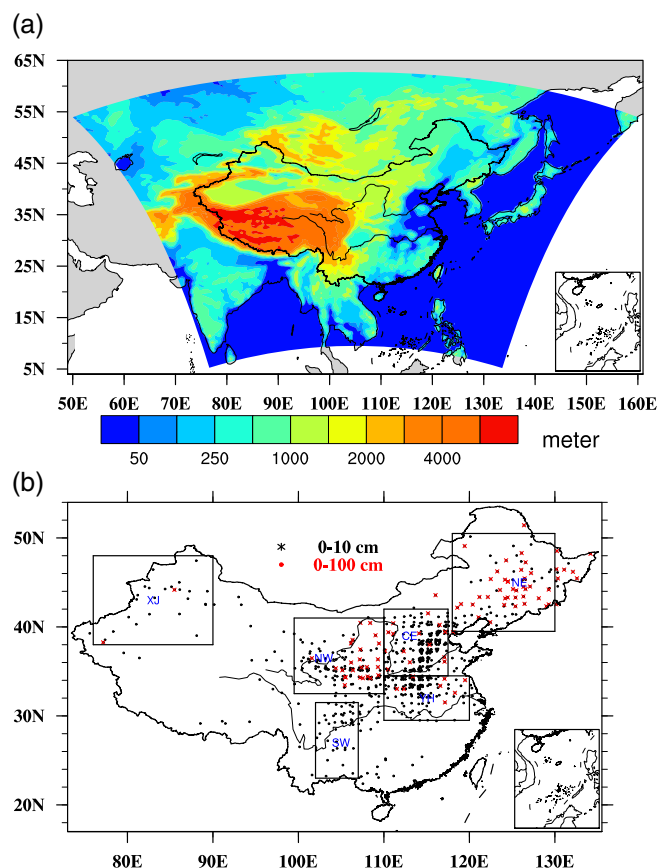


FIGURE 1 (a) Map of model domain with topography at a 50 km × 50 km horizontal resolution. (b) Distribution of in situ soil moisture stations used for the validation of model simulations. Black dots denote soil moisture available at 0–10 cm soil depth (732 stations), and red cross signs denote values collected from soil depths of 0–100 cm (96 stations). The boxes indicate the regional range with two-letter abbreviations provided for each region (XJ: 76°–90°E, 38°–48°N; NW: 99.5°–110°E, 32.5°–41°N; CE: 110°–117.5°E, 34.5°–42°N; NE: 118°–130°E, 39.5°–50.5°N; YH: 110°–120°E, 29.5°–34.5°N, and SW: 102°–107°E, 23°–31.5°N)

which was derived from the gravimetric method in China for the period of 1992–2013. This dataset includes the volumetric SM records for up to 732 stations in five soil layers (Figure 1b). The WS2019 datasets are used to validate the monthly model outputs for April to September of 1992–2010. The SM records in both 0–10 cm and 0–100 cm soil depths from the surface downward are adopted to compare with modelled values. The 0–10 cm layer represents the first soil layer in the NOAH LSM. The SM in this layer is directly affected by overlying atmospheric processes and shows concurrent variability with precipitation except for over arid regions (Wang and Shi, 2019). The SM within 0–100 cm soil depth is integrated the values from the upper three soil layers in NOAH LSM using the relative weights of each layer

thickness. That is, the SM in each soil layer multiples its layer thickness, then three products are added together, and the final SM within 0–100 cm soil depth is the ratio of above summation to the total thickness within upper three layers (i.e., 100 cm). The 0–100 cm soil depth accounts for majority vegetation root and SM deficiency in this depth is often used as an agricultural drought indicator (Wang *et al.*, 2011). Moreover, in order to perform the regional evaluation, the land area where majority SM stations locate is divided into six subregions following WS2019 (Figure 1b). The WRF simulated SM are also compared with regional mean observed SM over each subregion in Section 4.

3 | DROUGHT IDENTIFICATION

Since the soil water holding capacity and soil texture differ from region to region (e.g., Shangguan *et al.*, 2013), the magnitudes of SM (in volumetric form) is heterogeneous across space (Wang and Shi, 2019). Wang *et al.* (2009, 2011) converted the original model-simulated monthly SM to the percentile (SMP) time series with respect to its climatology for the same month during the study period and then successfully applied the SMP datasets to identify drought in the continental United States and China, respectively. The SMP magnitudes in all land pixels are within range of 1–100%, facilitating the comparisons among different climatic regimes and periods. Similar approach has been used in other studies (e.g., Sheffield *et al.*, 2009). Moreover, the SMP removes the effect of seasonal cycles and allows drought analyses to focus on the variations of interannual or longer time scales. In previous studies (Sheffield *et al.*, 2009; Wang *et al.*, 2009, 2011), the occurrence of drought is defined as that SMP is equal to or less than 20% at each grid cell, which implies that drought would have a 5-year return period if the time series of SMP is evenly distributed during 100 years. Reducing this threshold would lengthen the drought return period.

The identification of drought during a given period is usually based on four parameters: drought number (Dr), duration (Du), frequency (Fq), and severity (Sv). As in Wang *et al.* (2009, 2011) and Wang and Zeng (2018), at each land pixel, a drought event is defined as consecutive months under drought ($SMP \leq 20\%$) and Dr is the total number of drought events occurring during the study period. Du is the number of months that a drought event lasts for, Sv is the mean deficiency of the SMP in regard to the drought threshold [$Sv = \Sigma(1 - SMP/20\%)/Du$], and Fq is the reciprocal of the number of consecutive months without drought and represents intervals between two adjacent drought events. For each land pixel, we measure

Dr and then constructed the time series of Du, Sv and Fq during the study period. The spatial and temporal characteristics of these drought parameters are extensively analysed in the following sections.

4 | EVALUATION OF SOIL MOISTURE SIMULATIONS FROM WRF

Much research has demonstrated that multimodel ensemble simulations perform better than individual model experiment in terms of monthly quantities due to their offset noises and enhance signals especially for longer time periods (Guo *et al.*, 2007; Wang *et al.*, 2011; Crow *et al.*, 2012; Xia *et al.*, 2014). In this study, the monthly SM average from two experiments (refereed as to WRF-ENS) are computed and compared with the observation. Due to highly spatial heterogeneity and point-versus-grid cell mismatching, the comparison of point SM measurements and modelled grid box averages is always challenging. To partly avoid this problem, two approaches are adopted: (a) we use the average from observations at all stations in China (rather than focusing on an individual station) to compare the mean modelled values at all corresponding station locations (e.g., Wang and Zeng, 2011); and (b) we use the average from stations over six subregions (Wang and Shi, 2019) to compare the regional mean of model simulations (e.g., Xia *et al.*, 2014). For method 1, three modelled SM products (WRF-ERA20C, WRF-20CR, and WRF-ENS) from the original grid points are firstly interpolated to the station locations (Figure 1b) using the inverse distance weighted algorithm. Noted that, using different interpolation methods might affect the SM absolute quantity slightly but not the evaluation results. Because the in situ observed SM dataset contains missing records, the modelled SM products are spatial and temporal continuously. To perform a fair comparison, the modelled SM values are masked by available observations for each station. That is, if the observed record is missing at a station for a given month, the modelled SM is also set as the missing value. This process slightly affects the long-term mean of modelled SM. In contrast to method 1, method 2 emphasizes the regional representation of the dataset and avoids generating interpolation errors. It also reduces biases across different measurement points and has been used in numerous studies (e.g., Crow *et al.*, 2012; Xia *et al.*, 2014; Yuan and Quiring, 2017). Because the SM absolute magnitude varies dramatically across climate regimes and SM drought reflects relative SM deficiency with respect to the climatology mean for the study period, the anomalous SM is preferable for drought

FIGURE 2 Time series of monthly soil moisture ($\text{cm}^3 \cdot \text{cm}^{-3}$) over China for 1992–2010 at soil layers of (a) 0–10 cm and (b) 0–100 cm. Monthly values are averaged over data collected at 732 stations at 0–10 cm depth and 110 stations at 0–100 cm depth from observations (OBS) and simulations of WRF-ERA20C, WRF-20CR, and WRF-ENS. Only datasets for April to September of each year are plotted

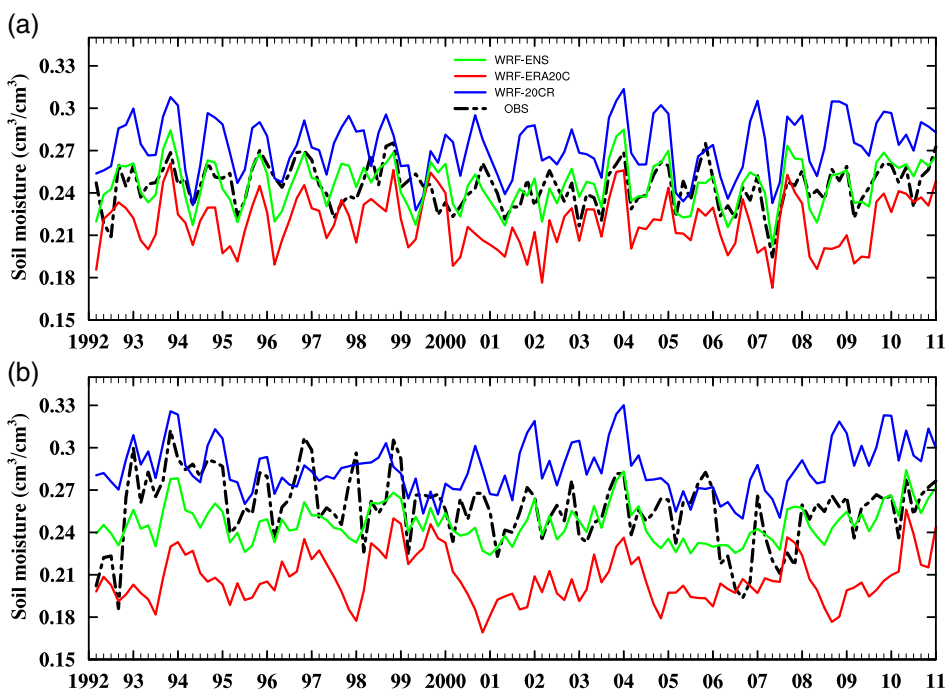


TABLE 1 Correlation coefficient (R) and root mean square error (RMSE, $\text{cm}^3 \cdot \text{cm}^{-3}$) between WRF-simulated SM and observations averaged across all available stations (Figure 1b). The monthly SM from WRF-20CR, WRF-ERA20C, WRF-ENS and station observations made in multiple growing seasons (April–September) for 1992–2010 are used to compute the statistical quantities. SM data for both 0–10 cm and 0–100 cm are analysed. Statistical values shown in bold represent the best simulations performed among the three simulations for each soil layer

	WRF-20CR		WRF-ERA20C		WRF-ENS	
	0–10 cm	0–100 cm	0–10 cm	0–100 cm	0–10 cm	0–100 cm
R	0.51	0.53	0.50	0.23	0.58	0.50
RMSE	0.033	0.034	0.030	0.057	0.015	0.026

analyses. Thus, we also compare the anomalous SM values derived from simulations and observations by extracting its monthly climatology at each station.

Figure 2 shows the monthly averaged SM over all available stations from observation (OBS) and three modelled products (referred to as method 1). As in Figure 2, the monthly SM anomalies are shown in Figure S1. Three WRF-derived SM products display similarly variability as the observation. The magnitude of SM is apparently overestimated/underestimated by WRF-20CR/WRF-ERA20C while the SM from WRF-ENS is overall in better agreement with OBS, especially for SM at 0–10 cm soil depth. The mean SM for the 0–10 cm soil layer is 0.24, 0.27, 0.22 and $0.25 \text{ cm}^3 \cdot \text{cm}^{-3}$ for OBS, WRF-20CR, WRF-ERA20C and WRF-ENS, respectively. We also computed the correlation coefficient (R) and root mean square error (RMSE) between the modelled SM and observations (Table 1). In the 0–10 cm soil layer, WRF-ENS produces the largest

R (0.60) and the smallest RMSE ($0.015 \text{ cm}^3 \cdot \text{cm}^{-3}$). The statistical values derived from the other two products are similar (R/RMSE is $0.51/0.033 \text{ cm}^3 \cdot \text{cm}^{-3}$ for WRF-20CR and $0.50/0.030 \text{ cm}^3 \cdot \text{cm}^{-3}$ for WRF-ERA20C). In the 0–100 cm soil layer, the R derived from WRF-ENS (0.50) is slightly smaller than that derived from WRF-20CR (0.53), and they are both larger than that derived from ERA-20C (0.23). The RMSE derived from WRF-ENS ($0.026 \text{ cm}^3 \cdot \text{cm}^{-3}$) is still smaller than those of the other two products, although they are larger than those derived from the SM in the shallow soil layer.

Figure 3 shows R and RMSE values of the three modelled products against the observations for six sub-regions. The monthly anomalous SM time series are also plotted (Figures S2 and S3). For SM in the 0–10 cm soil layer, R varies from 0.65 (WRF-ENS in XJ) to 0.14 (WRF-ERA20C in YH). For six subregions and three products, there are total 18 R/RMSE values. For SM in 0–10 cm soil layer (Figure 3a), all 18 R values are

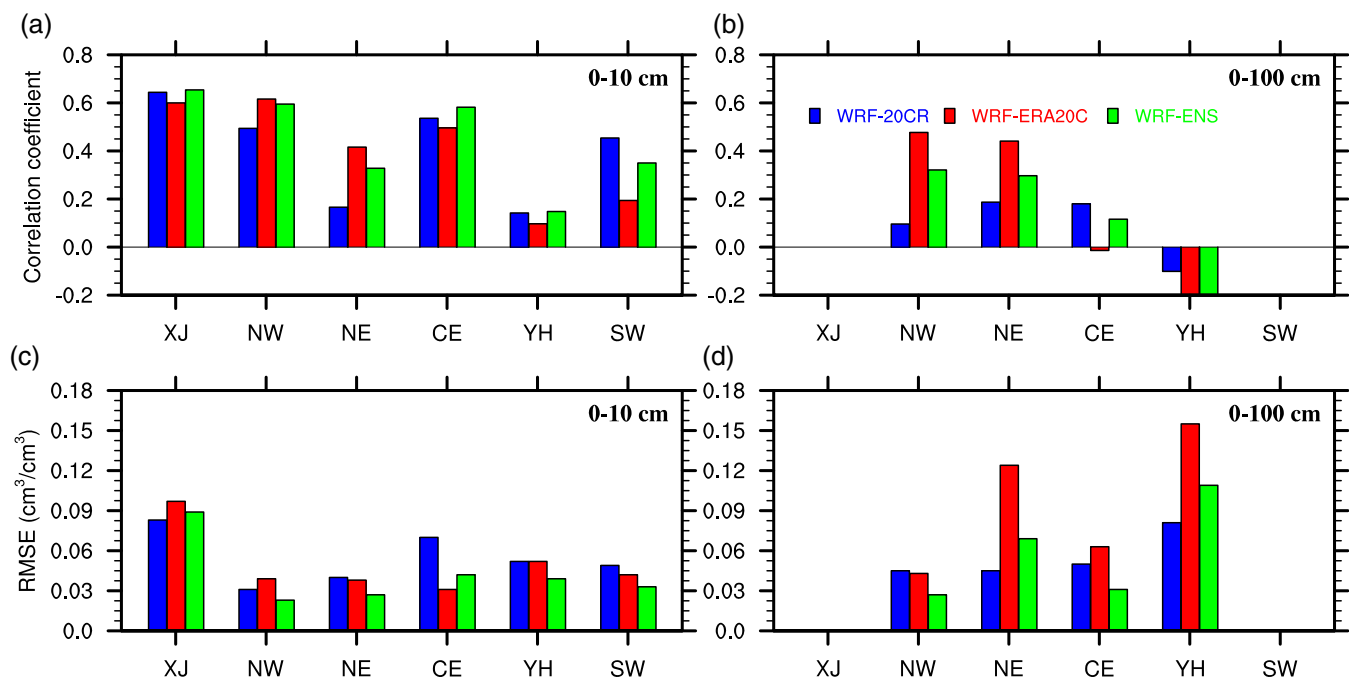


FIGURE 3 Regional comparison of the correlation coefficient (a and b) and root mean square error (RMSE, c and d) of soil moisture at 0–10 cm (a and c) and 0–100 cm (b and d) soil layers from WRF simulations and observations for 1992–2010. Regional divisions are shown in Figure 1b. Only data for April to September of each year are used to compute statistical quantities

positive with 16 of them are passing a significance test ($p < .05$), indicating good capability for WRF to reproduce SM in the shallow soil layer. The highest R appears in XJ and its lowest value is found in YH. Compared to two individual model experiments, WRF-ENS is better performed in terms of two statistical quantities. Its R is larger than that derived from the other two products for five (four) of the six subregions while its RMSE is the lowest one across the five subregions except for YH. For SM in the 0–100 cm soil layer, due to an absence of available observations for XJ and SW, statistical quantities are only computed for four subregions. Relative to the quantities observed in the shallow soil layer, the R decreases and even becomes negative, but the RMSE increases. In all four subregions, WRF-ENS overall presents a moderate R magnitude with a much lower RMSE in half of the subregions. Similar results have been reported from offline land surface modelling experiments (e.g., Xia *et al.*, 2014), and the model parameterization scheme for water transfer between soil layers is responsible for such results. The above results further reinforce this conclusion from the modelling experiments of NOAH LSM, guiding the direction of future LSM development. It should be noted that the regional mean of SM observations for the 0–100 cm soil layer might not be representative in some subregions (e.g., XJ) where available observations are too limited.

Because the two experiments are only different from the lateral boundary conditions, intercomparisons made among the three modelled results indicate strong effects of the lateral boundary conditions on the simulated SM. Moreover, as we noted above, the SM at 0–100 cm soil depth is preferable for vegetation growth and this is where majority roots are located (Zeng, 2001). According to the above evaluations and considerations, the monthly SM at the 0–100 cm soil depth from WRF-ENS (for simplicity, it is still referred to as SM in the following sections) is adopted to perform drought analyses in this manuscript.

5 | CENTURY-LONG SOIL MOISTURE DROUGHT ANALYSES FOR CHINA

5.1 | Spatial and temporal variations of a century-long soil moisture from WRF-ENS

Before long-term SM drought was analysed for China, we examined the spatial and temporal variabilities in the simulated SM from WRF-ENS for 1911–2010. At each grid cell, the monthly SM was first intergraded into the annual value, which was then used to compute the long-term annual mean and trend and interannual variability.

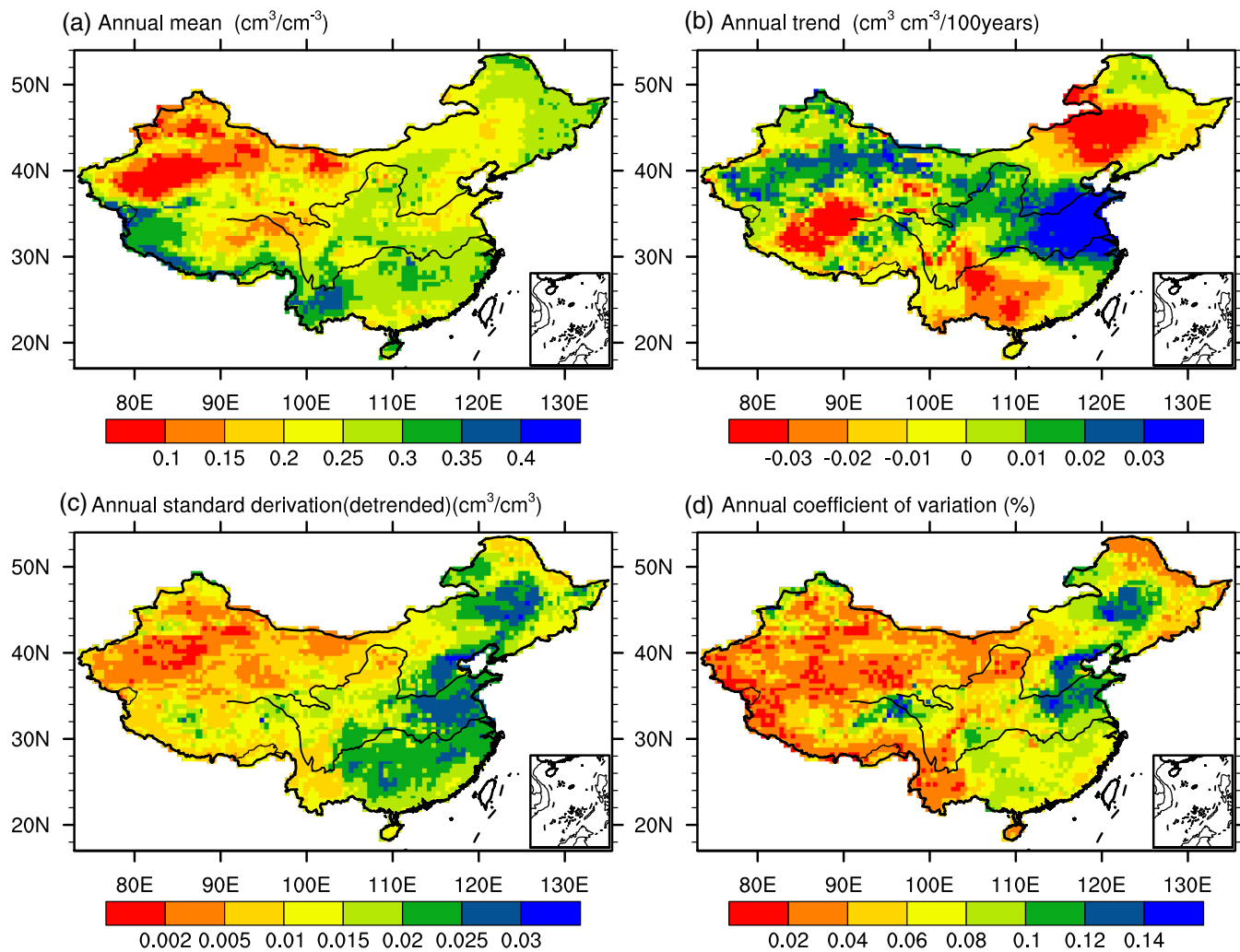


FIGURE 4 Soil moisture in the 0–100 cm soil layer over China for 1992–2010 for the (a) annual mean ($\text{cm}^3 \cdot \text{cm}^{-3}$), (b) annual linear trend ($\text{cm}^3 \cdot \text{cm}^{-3} \cdot 100 \text{ years}^{-1}$), (c) annual detrended SD ($\text{cm}^3 \cdot \text{cm}^{-3}$), and (d) coefficient of variation (%). The annual soil moisture (WRF-ENS) value is derived from the ensemble average of WRF-ERA20C and WRF-20CR

While the annual SM shows a similar spatial pattern as precipitation (figure not shown), its magnitudes are relatively large in southern and eastern China and small in the northwest and the Three-River Headwaters region (Figure 4a). The annual mean SM varies from 0.05 to $0.42 \text{ cm}^3 \cdot \text{cm}^{-3}$ across continental China. The areal averaged annual value and standard deviation (STD) are 0.24 and $0.015 \text{ cm}^3 \cdot \text{cm}^{-3}$ across all grid cells in China, respectively. Changes in SM in a specific region are mainly determined by surface meteorological variables (e.g., Wang and Zeng, 2011) and are also shaped by vegetation and soil parameters such as soil hydraulic conductivity and soil porosity (Shangguan *et al.*, 2013). The available moisture within a certain soil layer is confined by the field capacity of this layer and is usually lower than $0.5 \text{ cm}^3 \cdot \text{cm}^{-3}$ but varies with soil textures. Therefore, although the spatial pattern of annual SM roughly resembles precipitation across the whole country, SM also

exhibits its regional and local properties (Wang and Shi, 2019).

For a centennial SM dataset, a trend analysis is necessary to identify temporal change for different regions (Figure 4b). The linear trend of SM shows apparently spatial patterns across the whole country. Areas with apparent uptrends ($>0.03 \text{ cm}^3 \cdot \text{cm}^{-3} \cdot \text{year}^{-1}$) locate in lower reaches between the Yangtze and Yellow River Basins and Northwest China while three distinct downtrend centres ($<-0.03 \text{ cm}^3 \cdot \text{cm}^{-3} \cdot \text{year}^{-1}$) appear in the northeast, southern China, and the western Tibetan Plateau. The negative average trend for whole China mainland of $-1.2 \times 10^{-3} \text{ cm}^3 \cdot \text{cm}^{-3} \cdot \text{year}^{-1}$ indicates an overall pattern of drying soil for the study period.

To investigate the interannual variability in SM during the 100-year period, we computed the STD based on a detrend annual SM time series for each grid cell (Figure 4c). The STD shows distinctly regional variations

and its magnitude increases from west to east and from north to south in eastern China. A relatively large STD magnitude ($>0.02 \text{ cm}^3 \cdot \text{cm}^{-3}$) appears in part of the northeast, the central east and a large area in southern China. Because the STD somehow depends on the value of the absolute magnitude of SM, which is strongly regionally dependent, the coefficient of variation (CV), defined as the ratio of STD to the mean, can better illustrate the interannual variabilities in SM across different regions (Figure 4d). The CV pattern resembles that of STD, but its regional dependence is not as distinct as that of the STD. The maximum CV centres ($\text{CV} > 12\%$) in the northeast in low reaches of the Yellow River Basin, indicating relatively larger interannual variability in SM across those regions. This could be explained by the variations of East Asian Monsoon system that plays a leading role in the interannual precipitation variation in eastern China (Ding *et al.*, 2018). Research on the SM variability

in China from the offline LSM simulations and remoted sensing observation in recent decades indicates overall downward trends of SM particularly over northern China (e.g., Cheng *et al.*, 2015; Chen *et al.* 2016). However, trend of SM depends on the time period of interest. The above results present the general spatiotemporal characteristics of SM from WRF-ENS during 100 years, which are used to construct the SMP for retrospective drought analyses in the following sections.

5.2 | Mean soil moisture drought characteristics

Figure 5 shows the spatial distribution of the mean number of droughts (Dr) and the three mean drought parameters (i.e., D_u , F_q , S_v) derived from the SMP for China for 1911–2010. Dr increases from northwest to southeast,

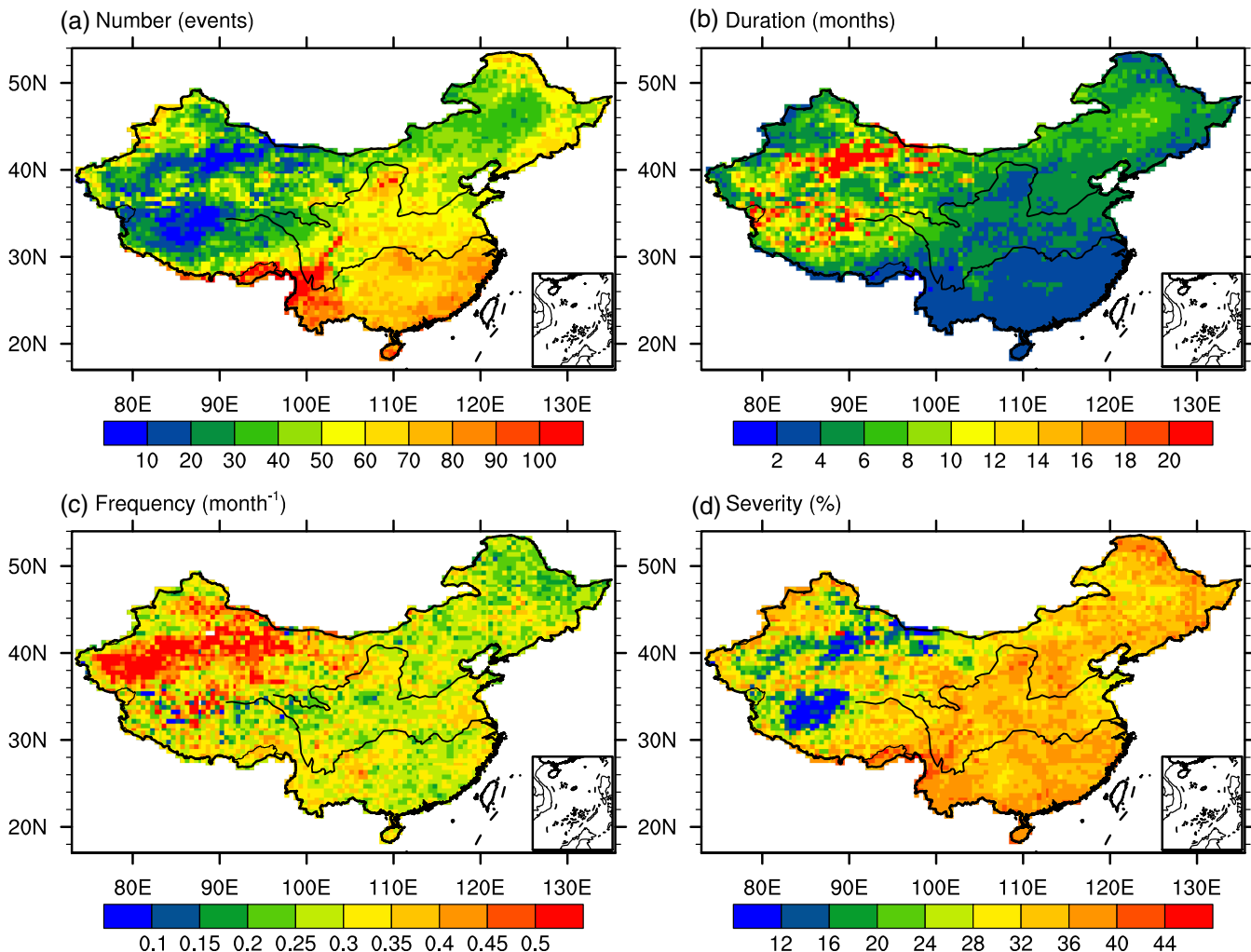


FIGURE 5 Map of drought parameters derived from the soil moisture percentile (SMP) for 1911–2010 over China: (a) drought number (events), (b) mean drought duration (months), (c) mean drought frequency (month^{-1}), and (d) mean drought severity (%). A drought event is defined as the SMP less than 20% for 1911–2010

and its maxima (more than 100 events) appears in Yunnan Province and in small border areas of the Tibetan Plateau (Figure 5a). Over the western Tibetan Plateau and Xinjiang Province, which represent arid regions of China, less than 10 drought events occur, but their mean Du are generally longer than 20 months, and their drought occurrences are also relatively frequent ($F_q > 0.5 \text{ month}^{-1}$). In contrast, in south China, the mean Du is generally less than 4 months, F_q is valued at $0.2\text{--}0.4 \text{ months}^{-1}$ and S_v ranges from 32 to 40%. In the northern China, the frequent occurrences of persistent multi-year droughts have been reported by analysing the observation-based drought indices (e.g., Yu *et al.*, 2014) and climate model simulations (e.g., Wang and Zeng, 2018). In contrast, previous researches also indicated that the short duration drought was preferably occurring in humid southern China (e.g., Wang *et al.*, 2016) where the high evaporation driven by the increased temperature leads to the desiccation of soil, but constant rainfall frequently replenishes water into the soil and relieves the soil dry condition. Therefore, a

general conclusion can be drawn: relatively prolonged droughts more easily occur in arid regions while short but frequent droughts are more likely to occur in humid regions.

5.3 | Spatial distribution of drought events of differing duration

To further investigate the occurrence of droughts in different regions, Figure 6 displays the distributions of the number of drought events (i.e., D_r) under different Du thresholds (≥ 3 , 6, 12, and 24 months, respectively) for the study period. Drought persistence for at least 3 months can occur anywhere in China, and its occurrence changes from less than two events in the northwest to more than 30 times in southwestern China (Figure 6a). With increasing Du thresholds, D_r increases from northwest to southwest. A prolonged drought with the Du longer than 24 months can only occur in the northwestern arid area, and the D_r is generally lower than 10 during

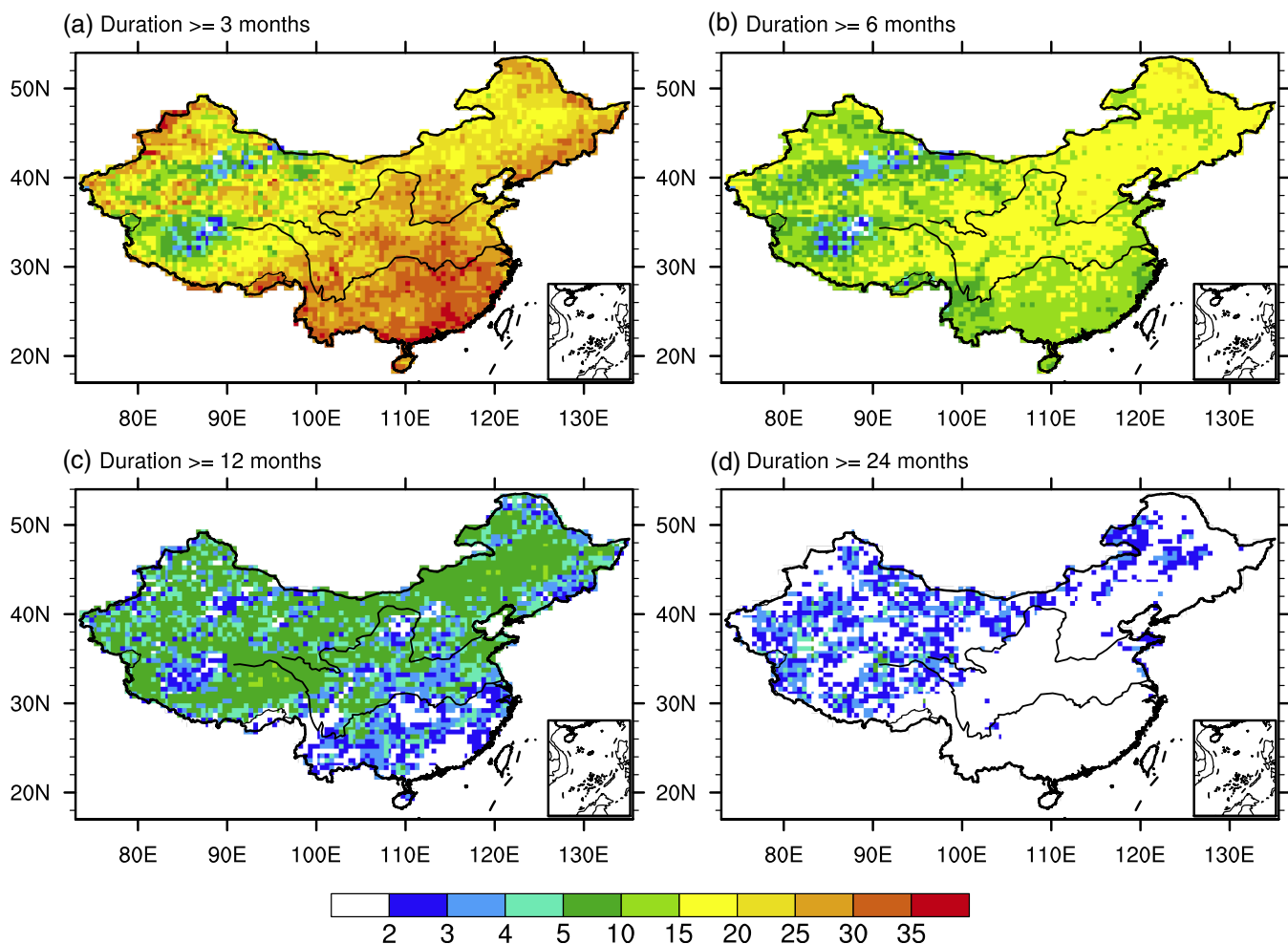


FIGURE 6 Occurrences of drought for durations at least (a) 3, (b) 6, (c) 12, and (d) 24 months for 1911–2010

the 100-year period (Figure 6d). Wang *et al.* (2016) reported that flash droughts are more frequent in humid and semi humid regions based on observation data analysis in China. Because the impacts of SM drought on agriculture and society may somehow rely on their duration, shorter droughts might cause less damage than longer ones.

5.4 | Long-term trends of drought characteristics in China

To explore long-term changes in SM drought patterns, the trends of three drought parameters for each grid are also computed using the Mann-Kendall (MK) nonparametric analysis algorithm (Mann, 1945). The MK test has been extensively used for testing monotonic trends in hydrometeorological time series (e.g., Wang *et al.*, 2011; Yu *et al.*, 2014; Cheng *et al.*, 2015;

Chen et al., 2016). Figure 7 plots the spatial distribution of grid cells with each drought parameter trend passing different significance level tests. All three drought parameters show distinctly downward trends in the lower reach areas between the Yangtze and Yellow River Basins and some scatter areas in northwest China. Intercomparisons of trend distributions of three drought parameters show that grid cells passing the significant level test are more scattered for Du and Sv than those for Fq. For Du and Sv, grid cells with significant upward and downward trends are staggered, implying their heterogenous properties across China's vast domain. For Fq, significant upward trends prevail over most areas of northern China, part of southern China and Yunnan Province, while grid cells with downward trends is mainly found in the lower reaches between the Yangtze and Yellow River Basin. The aggregation of land areas with significant trends ($p > 80\%$) shows that only 28.4, 28.9 and 38.4% of land areas present significant Du, Sv and Fq trends,

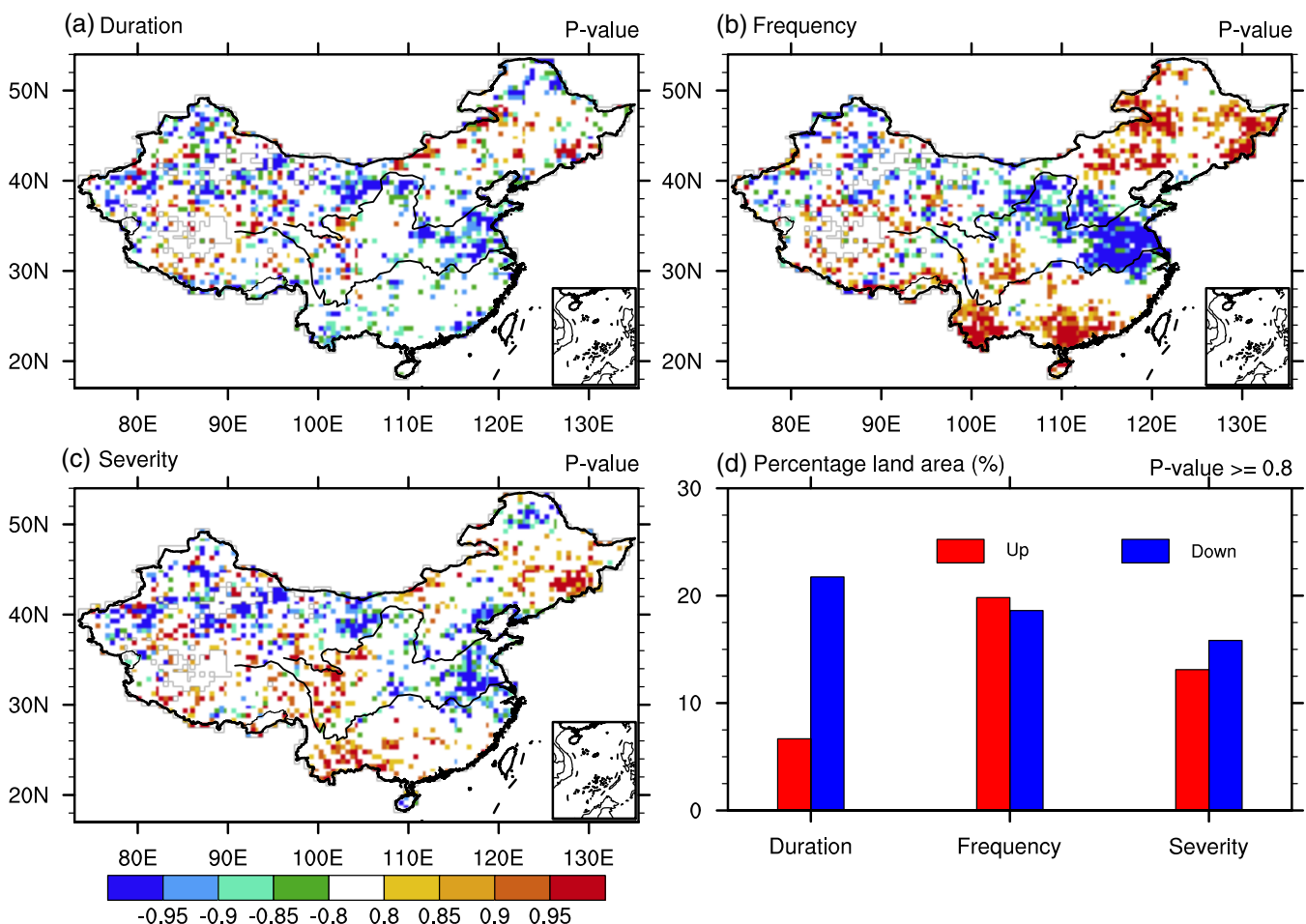


FIGURE 7 Mann-Kendall trends of drought parameters of (a) duration, (b) frequency, and (c) severity for 1911–2010. Values shown on the label bar denote the signed p -values for the significance of trends where a positive p -value indicates an uptrend while a negative p -value denotes as downtrend. (d) The percentage of land area showing drought characteristics with uptrends (red) and downtrends (blue) for p -value $\geq .8$.

respectively. Among these, land areas showing upward (downward) trend is 6.7% (21.7%) for Du, 13.1% (15.8%) for Sv, and 19.8% (18.6%) for Fq. Previous studies reported that dry land areas have expanded in recent several decades and drought has become more severe across China, especially in northeast China (Zhai *et al.*, 2010; Wang *et al.*, 2011; Cheng *et al.*, 2015). From current analysis, SM drought across China over a centurial long does not demonstrate an obviously drying tendency. The differences are largely attributed by the inconsistency of study periods, as well as the sources of dataset used to construct the drought index. Previous studies have also indicated that climate elements in China show distinctly multidecadal variabilities, partly due to decadal changes of the East Asian Summer Monsoon and changes in large-scale circulation patterns (Wang, 2001). These factors have also affected the variability of drought in China (Zhu *et al.* 2019).

5.5 | Multidecadal changes in SM drought variations

To investigate changes in SM drought in different periods, we computed drought parameter changes across different decades. We divided the last 90 years into three 30-year periods and then computed the drought parameters for each period. Changes in drought parameters for each pair of periods were then derived and plotted. Figure 8 shows the 30-year mean changes in drought parameters (Dr, Du, Fq and Sv) for 1981–2010 and 1921–1950 (figures for the differences between 1981–2010 and 1951–1980 and between 1951–1980 and 1911–1950 are shown in the supplemental materials, Figures S4 and S5). The Dr decreases in most areas from Xinjiang Province to Gansu Province and then to central eastern China but increases in vast areas of northeastern and southern China (including the Tibetan Plateau) and in small areas

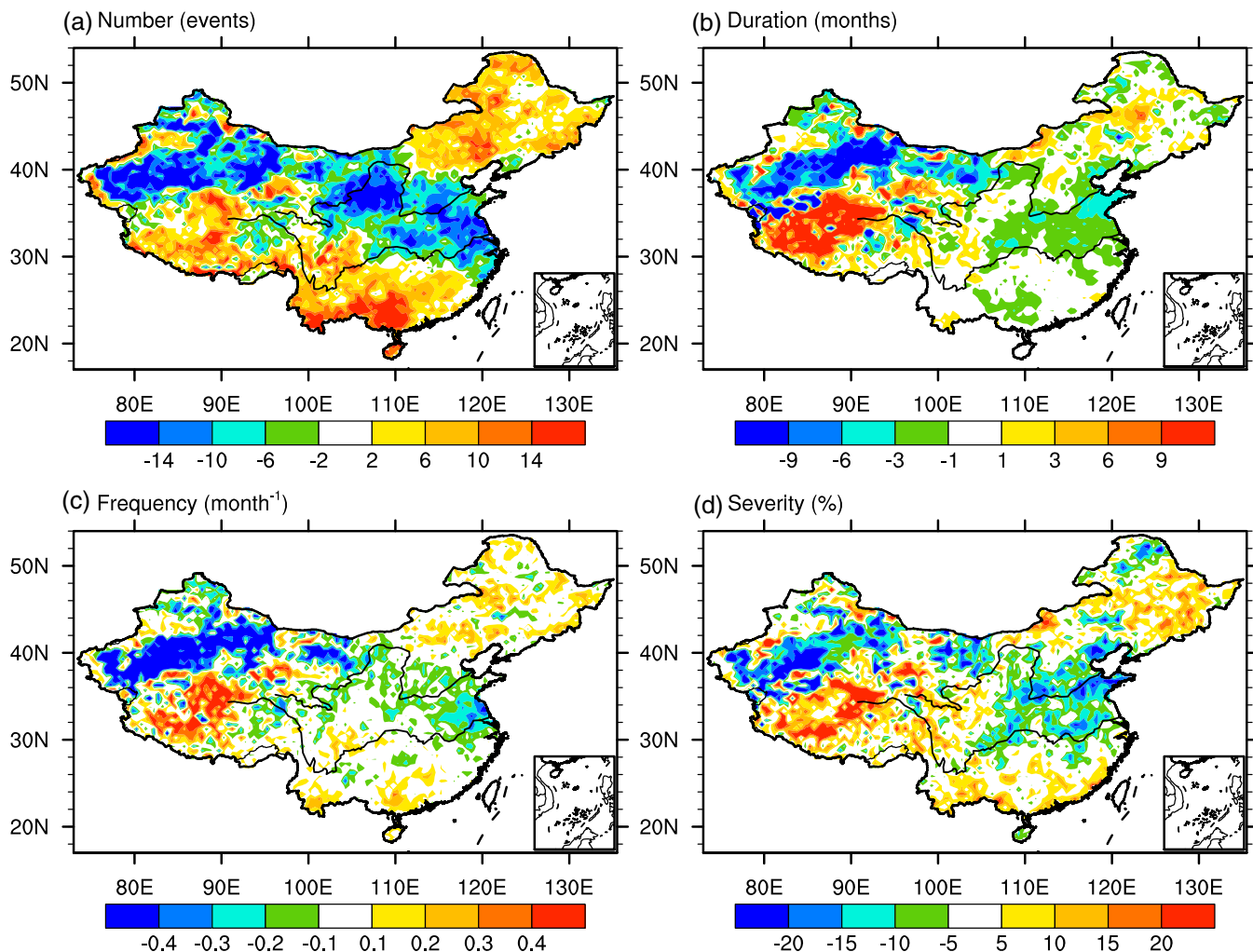


FIGURE 8 Differences in drought parameters observed between 1981–2010 and 1921–1950. (a) Drought number (events), (b) mean drought duration (months), (c) mean drought frequency (month^{-1}), and (d) mean drought severity (%)

of North Xinjiang Province (Figure 8a). Regarding the mean Du, positive change appears in the western Tibetan Plateau ($\Delta Du > 9$ months), but the opposite changes occur in central Xinjiang Province ($\Delta Du < -9$ months, Figure 8b). The spatial patterns of sign changes in both Fq and Sv are similar as that in Du Figure 8c,d.

To quantitatively illustrate changes in drought parameters, we firstly compute Dr and mean Du, Fq and Sv in each grid cell and period (i.e., 1921–1950, 1951–1980, and 1981–2010). To facilitate visualization and comparisons, we divide each drought parameter into different bins according to its magnitude and then integrate grid cell areas within each bin for each period. Finally, we plot the percentage of land area change versus drought parameter bins for three periods (Figure 9). More than 40% of land areas in China experience 10–20 drought events over 30-year periods, and areas for Dr within this bin during 1951–1980 are slightly smaller than those observed during the two other periods (Figure 9a). Regarding the mean Du, drought persisting for 3–6 months would occur in approximately 50% of the land area of China and longer duration (>12 months) events would occur in less than 10% of land areas (Figure 9b). Drought occurrences with a

mean Fq of 0.2–0.4 months⁻¹ are dominant and occur in more than 60% of the land area, while the percentage of land area experiencing higher frequency drought ($Fq > 0.4$ month⁻¹) decreases with time. Droughts with mean Sv values of 30–40% are dominant and occur in nearly 50% of land areas in all three periods.

The spatial pattern of drought characters in 1951–1980 is apparently different from those in other two periods (Figures S4 and S5). Compared to other two periods, the magnitudes of all four drought parameters distinctly decrease in Northwest China, and to a less extent, in lower reach area between Yangtze and Yellow River basins. This characteristic can also be seen in Figure 9. The long-term terrestrial drought is primarily attributed by the analogous changes of ocean–atmosphere circulation, which would cause changes of land moisture condition through teleconnection. Qian and Zhou (2014) has reported that the decadal change of North China aridity was related to the phase of pacific decadal oscillation (PDO) and three distinct PDO phase transition epochs during 1900–2010 are approximately consistent with three periods in current study. For example, our result shows less drought occurrences during 1951–1980 (Figures S4 and S5) when the PDO was in

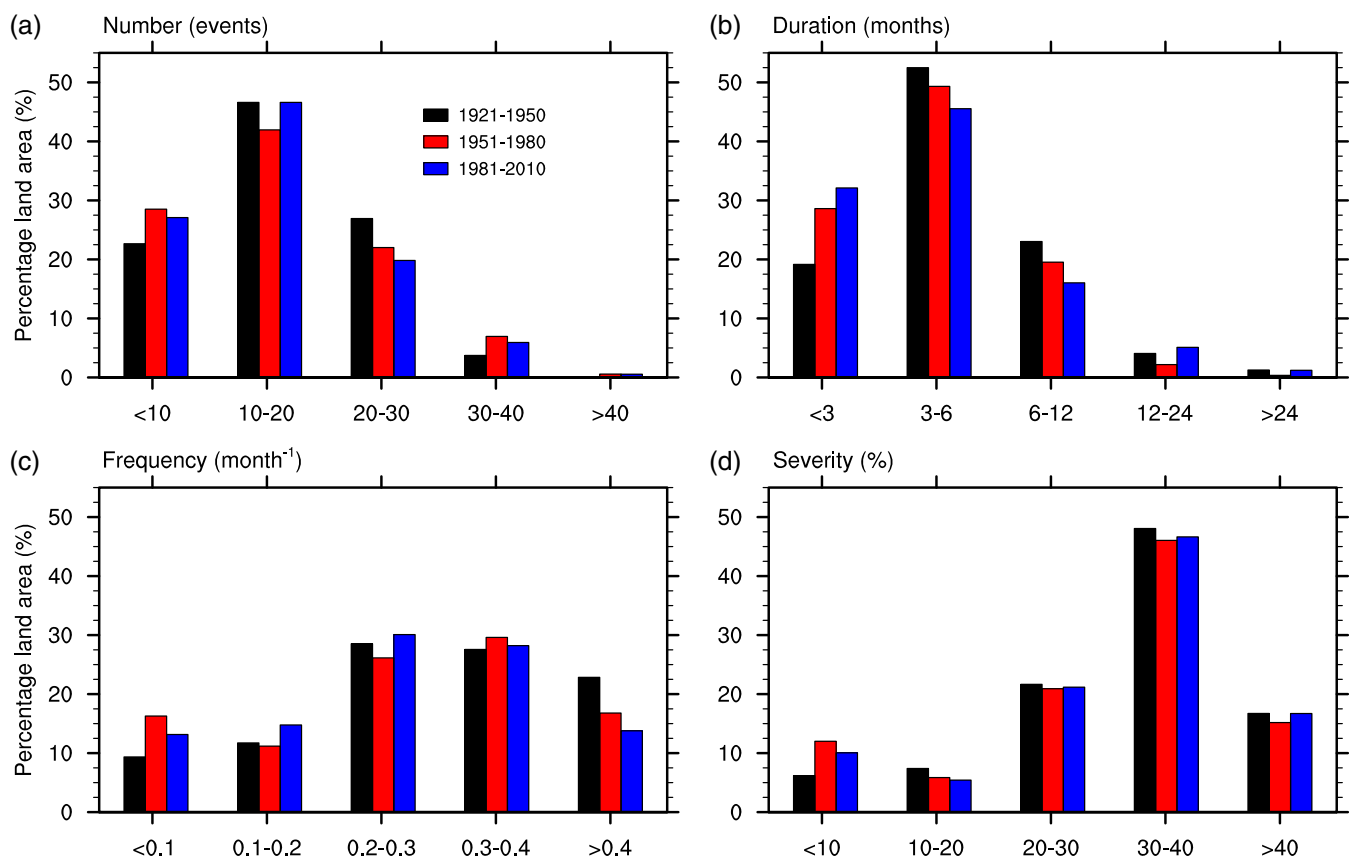


FIGURE 9 Percentage of land area showing drought parameters with different categories averaged over the periods of 1921–1950, 1951–1980, and 1981–2010. (a) Drought number (events), (b) mean drought duration (months), (c) mean drought frequency (month⁻¹), and (d) mean drought severity (%). The abscissa indicates the classification of each drought parameter, and the ordinate denotes the percentage of land area of each category

positive phase (Qian and Zhou, 2014). Besides, drought occurrences over different part of regions might be also linked to different largescale atmosphere–ocean circulation patterns, which will be further discussed in next section.

Although Figure 9 shows that the percentage of area within a specific bin for the same drought parameter changes slightly with time, the distributions of each bin in different periods do not change considerably. This result indicates that the distributions of accumulated land areas for individual drought parameter are independent of time periods regardless of their actual magnitude changing spatially in different time periods (Figure 8).

6 | CONCLUSION AND DISCUSSIONS

Of all forms of drought, drought induced by soil moisture (SM) deficiency has greatly impacted agriculture and water resources. In this study, we performed two WRF modelling experiments for 1901 to 2010 over the East Asia domain using the ERA-20C and 20CR as the lateral boundary conditions. The simulated monthly SM values for 1911–2010 were validated against in situ measurements made at multiple stations in China. The results indicate that the WRF model shows a certain capability to reproduce SM in China and that boundary conditions have greatly impacted SM simulations. The average SM drawn from two experiments exhibits better performance than that derived from individual ones in terms of temporal correlations, variability and biases. Considering the validation results and SM in agricultural practice, the monthly average SM for the 0–100 cm soil layer was used to construct a drought index (i.e., soil moisture percentile, SMP). With the definition of a drought event as successive monthly $SMP \leq 20\%$, we analysed spatiotemporal variabilities of number of events (Dr), duration (Du), severity (Sv) and frequency (Fq) during 100 years. Our main conclusions are as follows: (a) SM shows an increasing tendency along the belt from northwestern to central eastern China, while it displays clearly downtrends in the northeast, western Tibetan Plateau, and part of southeastern China. (b) The frequency of SM droughts increases from the northwestern (arid) to southeastern (humid) regions, mainly reflecting the spatial patterns of annual precipitation. SM drought events are generally prolonged and frequent (short intervals between two adjacent events) but less severe in arid regions (e.g., Xinjiang Province), while they are short, persistent (over 6-month periods), less frequent and more severe in humid regions (e.g., Yunnan Province). (c) During the centurial period, land areas showing significantly trend ($p > .8$) are only 28.4% for Du, 28.9% for Sv, and 38.4% for Fq, respectively.

Among them, the percentage of land areas showing downward trends for Du and Sv are generally larger than the percentage showing upward trends, indicating overall soil wetting tendency across China during 100 years.

It should be noted that changes in drought characteristics are strongly dependent on the time period of interest and the magnitudes of SM drought parameters. The latter ones are also determined by their thresholds. If different drought thresholds are adopted, these drought parameters might change in magnitude but not qualitatively. Furthermore, as noted in the introduction section, various drought indices have been constructed to emphasize different types of drought and do not necessarily show the same properties for the same regions. A SM drought event might not be consistent with a precipitation-based meteorological drought event occurring in arid regions in China (Wang and Shi, 2019). The mainland China covers different climate zones and its climate presents distinctly regional characteristics. The climate in east part is mainly impacted by the variability of the East Asian monsoon system, while in west part it is the typical arid and semiarid regions and its climate features hot and dry in summer and cold in winter. The decadal variations and regional characteristics in China's climate determinate the variability of drought (Wang, 2001; Cheng *et al.*, 2015; Zhu *et al.*, 2019). Although we have not addressed the causes of drought, the physical mechanisms of drought occurrences vary with regions and also related to the timescales. A review article of Zhang and Zhou (2015) indicated that drought in east China was linked to several atmosphere–ocean teleconnection patterns such as El Niño, the Pacific–Japan and Silk Road teleconnections, while in Northwest China the seasonal drought is related to northern Eurasian snow cover and is also impacted by the Tibetan Plateau through its effects on the atmospheric hydrological cycle and thermodynamics. Causes of drought in a specific region are usually resulted from the combination effects of several factors. Besides, soil moisture relies heavily on near surface climate variability, as is also modulated by the local vegetation cover and soil properties (Wang and Zeng, 2011). Note that we have not considered the land surface condition changes during the study period. Modelling studies have indicated that land use and land cover change would also influence the regional climate variability through the land-atmosphere interaction (e.g., Xu *et al.*, 2015).

Given the importance of long-term continuous land surface hydrology products in the regional climate research, the current work may represent the first attempt made to retrospectively run a regional climate model over a 100-year period in East Asia. As far as we know, this is also the first study to use WRF-simulated SM to investigate long-term drought patterns in China. The definition of drought parameters and analytical

methods used can also be applied in future studies. Moreover, because changes in SM are related to many processes occurring in land-climate systems, SM dataset creation is always a major challenge. Validations of modelled SM are usually limited due to a lack of reliable SM observations. Although we evaluated WRF-simulated SM against ground measurements at multiple stations for 1992–2010, there is still a lack of observations that assess the model simulations of earlier periods. On the other hand, the performance of WRF is also affected by model physical processes and their parameterization schemes (e.g., Gao *et al.*, 2011; Xue *et al.*, 2014). Therefore, to make better use of WRF-modelled SM, the development of validation datasets and enhancement model physical representations in terms of parameterization and numerical schemes must be emphasized.

ACKNOWLEDGMENTS

This work was supported by National Key Research and Development Project (2016YFA0602401) and two National Science Foundation of China (41925021 and 41875106). We thank for two anonymous reviewers' constructive comments.

ORCID

Aihui Wang  <https://orcid.org/0000-0002-4609-8774>

REFERENCES

- Below, R., Grover-Kopec, E. and Dilley, M. (2007) Documenting drought-related disasters: a global reassessment. *Journal of Environmental Research And Development*, 16(3), 328–344.
- Bonan, G. (2002) *Ecological Climatology: Concepts and Applications*, Vol. 678. Cambridge, England: Cambridge University Press.
- Chen, F. and Dudhia, J. (2001) Coupling an advanced land surface hydrology model with the Penn State-NCAR MM5 modeling system. Part I: model implementation and sensitivity. *Monthly Weather Review*, 129, 569–585.
- Chen, H. and Sun, J. (2017) Characterizing present and future drought changes over eastern China. *International Journal of Climatology*, 37, 138–156. <https://doi.org/10.1016/j.jhydrol.2016.11.044>.
- Chen, X., Su, Y., Liao, J., Shang, T., Dong, T., Wang, C. and Liu, L. (2016) Detecting significant decreasing trends of land surface soil moisture in eastern China during the past three decades (1979–2010). *Journal of Geophysical Research: Atmospheres*, 121(10), 5177–5192.
- Cheng, S., Guan Huang, X., Ji, F. and Guo, R. (2015) Long-term trend and variability of soil moisture over East Asia. *Journal of Geophysical Research – Atmospheres*, 120, 8658–8670. <https://doi.org/10.1002/2015JD023206>.
- Chou, M.D. and Suarez, M.J. (1999) *A solar radiation parameterization for atmospheric studies*. NASA Tech. Rep. NASA/TM-1999-10460, 15. Greenbelt, MD: NASA Goddard Space Flight Cent., p. 38.
- Comp, G.P. and Coauthors. (2011) The twentieth century reanalysis project. *Quarterly Journal of the Royal Meteorological Society*, 137, 1–28. <https://doi.org/10.1002/qj.776>.
- Crow, W.T., Kumar, S.V. and Bolten, J.D. (2012) On the utility of land surface models for agricultural drought monitoring. *Hydrology and Earth System Sciences*, 16, 3451–3460.
- Dai, A.G. (2011) Drought under global warming: a review. *Wiley Interdisciplinary Reviews: Climate Change*, 2(1), 45–65.
- Ding, Y., et al. (2018) On the characteristics, driving forces and inter-decadal variability of the East Asian summer monsoon. *Chinese Journal of Atmospheric Sciences (in Chinese)*, 42(3), 533–558. <https://doi.org/10.3878/j.issn.1006-9895.1712.17261>.
- Gao, X.J., et al. (2017) Performance of RegCM4 over major river basins in China. *Advances in Atmospheric Sciences*, 34(4), 441–455. <https://doi.org/10.1007/s00376-016-6179-7>.
- Gao, Y.H., Xue, Y.K., Peng, W., Kang, H.-S. and Waliser, D. (2011) Assessment of dynamic downscaling of the extreme rainfall over East Asia using regional climate model. *Advances in Atmospheric Sciences*, 28, 1077–1098.
- Giorgi, F. (2019) Thirty years of regional climate modeling: where are we and where are we going next? *Journal of Geophysical Research - Atmospheres*, 124, 5696–5723. <https://doi.org/10.1029/2018JD030094>.
- Guo, Z.C., Dirmeyer, P.A., Gao, X. and Zhao, M. (2007) Improving the quality of simulated soil moisture with a multi-model ensemble approach. *Quarterly Journal of the Royal Meteorological Society*, 133, 731–747.
- Gupta, A., Rico-Medina, A. and Cano-Delgado, I. (2020) The physiology of plant response to drought. *Science*, 368, 226–269.
- Han, J. and Pan, H.L. (2011) Revision of convection and vertical diffusion schemes in the NCEP Global Forecast System. *Weather and Forecasting*, 2, 520–533. <https://doi.org/10.1175/WAF-D-10-05038.1>.
- Hong, S.Y. and Lim, J.O.J. (2006) The WRF single-moment 6-class microphysics scheme (WSM6). *Journal of the Korean Meteorological Society*, 42, 129–151.
- Huang, J., Yu, H., Guan, X., Wang, G. and Guo, R. (2016) Accelerated dryland expansion under climate change. *Nature Climate Change*, 6, 166–171. <https://doi.org/10.1038/NCLIMATE2837>.
- Kong, X.H. and Bi, X.Q. (2015) Dynamical downscaling of the twentieth century reanalysis for China: climatic means during 1981–2010. *Atmospheric and Oceanic Science Letters*, 8, 166–173. <https://doi.org/10.3878/AOSL20140099>.
- Kong, X.H., Wang, A.H., Bi, X.Q. and Wang, D. (2019) Assessment of temperature extremes in China using RegCM4 and WRF. *Advances in Atmospheric Sciences*, 36(4), 363–377. <https://doi.org/10.1007/s00376-018-8144-0>.
- Liu, Y.W., Liu, Y.B. and Wang, W. (2019) Inter-comparison of satellite-retrieved and global land data assimilation system-simulated soil moisture datasets for global drought analysis. *Remote Sensing of Environment*, 220, 1–18. <https://doi.org/10.1016/j.rse.2018.10.026>.
- Liu, Y.Y., Parinussa, R.M., Dorigo, W.A., De Jeu, R., Wagner, W., Van Dijk, A., McCabe, M.F. and Evans, J. (2011) Developing an improved soil moisture dataset by blending passive and active microwave satellite-based retrievals. *Hydrology and Earth System Sciences*, 15, 425–436. <https://doi.org/10.5194/hess-15-425-2011>.

- Mann, H.B. (1945) Nonparametric tests again trend. *Econometrica*, 13, 245–259.
- Poli, P., et al. (2016) ERA-20C: an atmospheric reanalysis of the twentieth century. *Journal of Climate*, 29, 4083–4097. <https://doi.org/10.1175/JCLI-D-15-0556.1>.
- Qian, W., Hu, Q., Zhu, Y. and Lee, D.-K. (2003) Centennial-scale dry-wet variations in East Asia. *Climate Dynamics*, 21, 77–89. <https://doi.org/10.1007/s00382-003-0319-3>.
- Qian, C. and Zhou, T. (2014) Multidecadal variability of north China aridity and its relationship to PDO during 1900–2010. *Journal of Climate*, 27, 1210–1222. <http://doi.org/10.1175/JCLI-D-13-00235.1>.
- Redmond, K.L. (2002) The depiction of drought: a commentary. *Bulletin of the American Meteorological Society*, 83(8), 1143–1147.
- Rhee, J., Im, J. and Carbone, G.J. (2010) Monitoring agricultural drought for arid and humid regions using multi-sensor remote sensing data. *Remote Sensing of Environment*, 114, 2875–2887. <https://doi.org/10.1016/j.rse.2010.07.005>.
- Richards, L.A. (1931) Capillary conduction of liquids in porous mediums. *Physics*, 1, 318–333.
- Shangguan, W., Dai, Y., Duan, Q., Liu, B. and Yuan, H. (2013) A global soil data set for earth system modeling. *Journal of Advances in Modeling Earth Systems*, 6, 249–263. <https://doi.org/10.1002/jame.20026>
- Sheffield, J., Andreadis, K.M., Wood, E.F. and Lettenmaier, D.P. (2009) Global and continental drought in the second half of the twentieth century: severity-area-duration analysis and temporal variability of large-scale events. *Journal of Climate*, 22, 1962–1981.
- Shen, C.M., Wang, W.-C., Hao, Z.X. and Gong, W. (2007) Exceptional drought events over eastern China during the last five centuries. *Climate Change*, 85, 453–471.
- Skamarock, W. C., et al. (2008) A description of the advanced research WRF version 3. NCAR Tech. Note TN-475_STR, 113 pp.
- Spinoni, J., Vogt, J.V., Naumann, G., Barbosa, P. and Dosio, A. (2018) Will drought events become more frequent and severe in Europe? *International Journal of Climatology*, 38, 1718–1736.
- Su, B., et al. (2018) Drought losses in China might double between the 1.5°C and 2.0°C warming. *Proceedings of the National Academy of Sciences*, 115, 10600–10605.
- Sukoriansky, S., Galperin, B. and Perov, V. (2006) A quasi-normal scale elimination model of turbulence and its application to stably stratified flows. *Nonlinear Processes in Geophysics*, 13, 9–22. <https://doi.org/10.5194/npg-13-9-2006>.
- Sun, C. and Yang, S. (2012) Persistent severe drought in southern China during winter-spring 2011: large-scale circulation patterns and possible impacting factors. *Journal of Geophysical Research, [Atmospheres]*, 117, D10112. <https://doi.org/10.1029/2012JD017500>.
- Wang, A., Bohn, T., Mahanama, S., Koster, R. and Lettenmaier, D. (2009) Multimodel ensemble reconstruction of drought over the continental United States. *Journal of Climate*, 22, 2694–2712. <https://doi.org/10.1175/2008JCLI2586.1>.
- Wang, A., Lettenmaier, D. and Sheffield, J. (2011) Soil moisture drought in China, 1950–2006. *Journal of Climate*, 24, 3257–3270. <https://doi.org/10.1175/2011JCLI3733.1>.
- Wang, A. and Shi, X. (2019) A multilayer soil moisture dataset based on the gravimetric method in China and its characteristics. *Journal of Hydrometeorology*, 20, 1721–1736. <https://doi.org/10.1175/JHM-D-19-0035.1>.
- Wang, A. and Zeng, X. (2011) Sensitivities of terrestrial water cycle simulations to the variations of precipitation and air temperature in China. *Journal of Geophysical Research*, 116, D02107. <https://doi.org/10.1029/2010JD014659>.
- Wang, A. and Zeng, X. (2012) Evaluation of multi-reanalysis products with in situ observations over the Tibetan Plateau. *Journal of Geophysical Research*, 117, D05102. <https://doi.org/10.1029/2011JD016553>.
- Wang, A. and Zeng, X. (2018) Impacts of internal climate variability on meteorological drought changes in China. *Atmospheric and Oceanic Science Letters*, 11, 78–85. <https://doi.org/10.1080/16742834.2017.1379865>.
- Wang, G., Gong, T., Lu, J., Lou, D., Hagan, D. and Chen, T. (2018) On the long-term changes of drought over China (1948–2012) from different methods of potential evapotranspiration estimations. *International Journal of Climatology*, 38, 2954–2966.
- Wang, H.J. (2001) The weakening of the Asian monsoon circulation after the end of 1970's. *Advances in Atmospheric Sciences*, 18(3), 376–386.
- Wang, L.Y., Yuan, X., Xie, Z.H., Wu, P.L. and Li, Y.H. (2016) Increasing flash droughts over China during the recent global warming hiatus. *Scientific Reports*, 6, 30571. <https://doi.org/10.1038/srep30571>.
- Xia, Y., et al. (2014) Evaluation of multi-model simulated soil moisture in NLDAS-2. *Journal of Hydrology*, 512, 107–125.
- Xu, Z., Mahmood, R., Yang, Z.-L., Fu, C. and Su, H. (2015) Investigating diurnal and seasonal climatic response to land use and land cover change over monsoon Asia with the community earth system model. *Journal of Geophysical Research – Atmospheres*, 120, 1137–1152. <https://doi.org/10.1002/2014JD022479>.
- Xue, Y.K., Janjic, Z., Dudhia, J., Vasic, R. and De Sales, F. (2014) A review on regional dynamical downscaling in intraseasonal to seasonal simulation/prediction and major factors that affect downscaling ability. *Atmospheric Research*, 147/148(1–15), 68–85.
- Yang, K., and Coauthors (2013) A multiscale soil moisture and freeze-thaw monitoring network on the third pole. *Bulletin of the American Meteorological Society*, 94, 1907–1916. <https://doi.org/10.1175/BAMS-D-12-00203.1>.
- Yu, M., Li, Q., Hayes, M., Svobodab, M. and Heime, R. (2014) Are droughts becoming more frequent or severe in China based on the standardized precipitation evapotranspiration index: 1951–2010? *International Journal of Climatology*, 34, 545–558. <https://doi.org/10.1002/joc.3701>.
- Yuan, S. and Quiring, S.M. (2017) Evaluation of soil moisture in CMIP5 simulations over contiguous United States using in situ and satellite observations. *Hydrology and Earth System Sciences*, 21, 2203–2218. <https://doi.org/10.5194/hess-21-2203-2017>.
- Zeng, X.B. (2001) Global vegetation root distribution for land modeling. *Journal of Hydrometeorology*, 2, 525–530.
- Zhai, J., Su, B., Krysanova, V., Vetter, T., Gao, C. and Jiang, T. (2010) Spatial variation and trends in PDSI and SPI indices and their relation to streamflow in 10 large regions of China. *Journal of Climate*, 23, 649–663.
- Zhang, L. and Zhou, T. (2015) Drought over East Asia: A review. *Journal of Climate*, 28, 3375–3399.
- Zhu, Y.L., Liu, Y., Wang, H.J. and Sun, J.Q. (2019) Changes in the interannual summer drought variation along with the regime

shift over Northwest China in the late 1980s. *Journal of Geophysical Research, [Atmospheres]*, 124, 2868–2881.

SUPPORTING INFORMATION

Additional supporting information may be found online in the Supporting Information section at the end of this article.

How to cite this article: Wang A, Kong X.

Regional climate model simulation of soil moisture and its application in drought reconstruction across China from 1911 to 2010. *Int J Climatol.* 2021;41 (Suppl. 1):E1028–E1044. <https://doi.org/10.1002/joc.6748>